



Comprehensive Analysis of Transcriptome-wide m⁶A Methylome Upon *Clostridium perfringens* Beta2 Toxin Exposure in Porcine Intestinal Epithelial Cells by m⁶A Sequencing

Juanli Zhang¹, Qiaoli Yang¹, Jiaojiao Yang¹, Xiaoli Gao¹, Ruirui Luo¹, Xiaoyu Huang¹, Zunqiang Yan¹, Pengfei Wang¹, Wei Wang¹, Kaihui Xie¹, Bo Zhang¹ and Shuangbao Gun^{1,2*}

¹College of Animal Science and Technology, Gansu Agricultural University, Lanzhou, China, ²Gansu Research Center for Swine Production Engineering and Technology, Lanzhou, China

OPEN ACCESS

Edited by:

George E. Liu,
Agricultural Research Service (USDA),
United States

Reviewed by:

Narendra Singh,
Stowers Institute for Medical
Research, United States
Eveline M Ibeagha-Awemu,
Agriculture and Agri-Food Canada
(AAFC), Canada

*Correspondence:

Shuangbao Gun
gunsbao056@126.com

Specialty section:

This article was submitted to
Epigenomics and Epigenetics,
a section of the journal
Frontiers in Genetics

Received: 01 April 2021

Accepted: 30 September 2021

Published: 19 October 2021

Citation:

Zhang J, Yang Q, Yang J, Gao X,
Luo R, Huang X, Yan Z, Wang P,
Wang W, Xie K, Zhang B and Gun S
(2021) Comprehensive Analysis of
Transcriptome-wide m⁶A Methylome
Upon *Clostridium perfringens* Beta2
Toxin Exposure in Porcine Intestinal
Epithelial Cells by m⁶A Sequencing.
Front. Genet. 12:689748.
doi: 10.3389/fgene.2021.689748

Piglet diarrhea is a swine disease responsible for serious economic impacts in the pig industry. *Clostridium perfringens* beta2 toxin (CPB2), which is a major toxin of *C. perfringens* type C, may cause intestinal diseases in many domestic animals. N⁶-methyladenosine (m⁶A) RNA methylation plays critical roles in many immune and inflammatory diseases in livestock and other animals. However, the role of m⁶A methylation in porcine intestinal epithelial (IPEC-J2) cells exposed to CPB2 has not been studied. To address this issue, we treated IPEC-J2 cells with CPB2 toxin and then quantified methylation-related enzyme expression by RT-qPCR and assessed the m⁶A methylation status of the samples by colorimetric N⁶-methyladenosine quantification. The results showed that the methylation enzymes changed to varying degrees while the m⁶A methylation level increased ($p < 0.01$). On this basis, we performed N⁶-methyladenosine sequencing (m⁶A-seq) and RNA sequencing (RNA-seq) to examine the detailed m⁶A modifications and gene expression of the IPEC-J2 cells following CPB2 toxin exposure. Our results indicated that 1,448 m⁶A modification sites, including 437 up-regulated and 1,011 down-regulated, differed significantly between CPB2 toxin exposed cells and non-exposed cells ($p < 0.05$). KEGG pathway analysis results showed that m⁶A peaks up-regulated genes ($n = 394$) were mainly enriched in cancer, Cushing syndrome and Wnt signaling pathways, while m⁶A peaks down-regulated genes ($n = 920$) were mainly associated with apoptosis, small cell lung cancer, and the herpes simplex virus 1 infection signaling pathway. Furthermore, gene expression (RNA-seq data) analysis identified 1,636 differentially expressed genes (DEGs), of which 1,094 were up-regulated and 542 were down-regulated in the toxin exposed group compared with the control group. In addition, the down-regulated genes were involved in the Hippo and Wnt signaling pathways. Interestingly, the combined results of m⁶A-seq and RNA-seq identified genes with up-regulated m⁶A peaks but with down-regulated expression, here referred to as “hyper-down” genes ($n = 18$), which were mainly enriched in the Wnt signaling pathway. Therefore, we speculate that the genes in the Wnt signaling pathway may be modified by m⁶A methylation in CPB2-induced IPEC-J2 cells. These findings

provide new insights enabling further exploration of the mechanisms underlying piglet diarrhea caused by CPB2 toxin.

Keywords: m⁶A-seq, RNA-seq, beta2 toxin, M⁶A modification, porcine intestinal epithelial cells

INTRODUCTION

Clostridium perfringens, which is one of the most important zoonotic pathogens (Immerseel et al., 2005), can cause severe bleeding ulcers and mucosal necrosis of the small intestine in humans and animals. It can produce four main toxins (α , β , ϵ , ι), according to which it is divided into five types: A, B, C, D, and E (Garcia et al., 2012). The *C. perfringens* beta2 (CPB2) toxin was first discovered in the supernatant of a culture of *C. perfringens* type C by Gibert et al. (1997). Its protein molecular weight is 28 kDa, with an isoelectric point of 5.4–5.5, and it is associated with gastrointestinal diseases in livestock caused by *C. perfringens*. The effect of CPB2 toxin on intestinal membrane epithelial cells indicates that it is strongly cytotoxic. When a low concentration of the toxin is introduced into these cells, the cells become rounded and damaged (Gibert et al., 1997). However, the mechanism by which CPB2 toxin induces diarrhea in animals (especially pigs) is still unclear and should be further studied.

N⁶-methyladenosine (m⁶A) modification is pervasive within mRNA and plays important regulatory roles in various biological processes (Meyer et al., 2012). In mammalian species, about one-third of mRNAs are modified by m⁶A (average of three to five m⁶A modifications in each mRNA), and many m⁶A sites are evolutionarily conserved between humans and mice (Huang et al., 2020). Dominissini et al. (2012) used m⁶A-specific antibodies to enrich fragments containing m⁶A and to identify the expression of m⁶A in whole transcripts of humans and mice by a high-throughput sequencing method (MeRIP-seq). m⁶A is mainly located near the termination codons and 3'UTRs of mRNA, and can influence pre-mRNA splicing (Zhao et al., 2014; Xiao et al., 2016), RNA structure (Liu et al., 2015), nuclear mRNA (Fustin et al., 2013), miRNA maturation (Alarcón et al., 2015), mRNA stability (Huang et al., 2018), chromosome inactivation (Patil et al., 2016), mRNA translation (Shi et al., 2017), and even RNA degradation (Zhu et al., 2014).

m⁶A modification plays very important roles in various immune and inflammatory responses to bacterial infection, such as the inflammatory response of human dental pulp cells (HDPCs) induced by lipopolysaccharide (LPS) (Feng et al., 2018) and the response of porcine small intestinal epithelial (IPEC-J2) cells to *Escherichia coli* K88 infection (Zong et al., 2018). In addition, Wu et al. (2020) found that deletion of YTH domain family 2 (YTHDF2) in the m⁶A reader promotes the demethylation of histone H3 lysine-27 trimethylation (H3K27me3) modifications, which in turn increases proinflammatory cytokine levels. However, the role of m⁶A modification in IPEC-J2 cells exposed to CPB2 remains unclear. Therefore, to better understand m⁶A modification in response to CPB2 toxin exposure, we performed N⁶-methyladenosine sequencing (m⁶A-seq) and RNA sequencing

(RNA-seq) to investigate differentially methylated genes (DMGs) and differentially expressed genes (DEGs) in IPEC-J2 cells that were exposed to CPB2. Our results provide a theoretical basis for further research into the molecular mechanisms of m⁶A modification in IPEC-J2 cells exposed to CPB2.

MATERIALS AND METHODS

CPB2 Toxin Extraction and Purification

The extraction and purification of CPB2 toxin were performed according to the method described by Luo et al. (2020). Briefly, a recombinant plasmid containing the CPB2 gene was successfully constructed and transformed into *E. coli* BL21 competent cells. Then, a single colony was selected, placed in medium containing kanamycin and incubated for 2.5 h at 37°C and 220 rpm. When the optical density (OD) reached 0.5–0.8, 1 mM isopropyl β -D-1-thiogalactopyranoside (IPTG, Solarbio, Beijing, China) was added to induce the bacteria at 16°C for 12 h. The precipitates were collected and suspended in 20 mM Tris-HCl buffer (pH 8.0), sonicated on ice, and purified by using High-Affinity Ni-Charged Resin FF (GenScript, Nanjing, China). The resin was washed with 10 mM imidazole lysis buffer and then eluted with 250 and 500 mM imidazole. Recombinant protein expression was detected by 12% alkyl sulfate-polyacrylamide gel electrophoresis (SDS-PAGE). Next, 10 mL of protein sample was loaded into a membrane and purified by dialysis against 1 × PBS (pH 7.6) for 24 h, then concentrated with PEG6000 for 40 min. Finally, Endotoxin Erasol (Genscript, Nanjing, China) was used to remove endotoxins.

Cell Culture

IPEC-J2 cells were provided by the Beijing Beina Chuanglian Institute of Biotechnology (Beijing, China) and cultured in 90% Dulbecco's modified Eagle's medium (DMEM, HyClone, Logan, United States) with 10% fetal bovine serum (FBS, HyClone), penicillin (100 U/mL), and streptomycin (100 μ g/mL) at 37°C in a 5% CO₂ atmosphere. The medium was changed every 2 days, and the cells were passaged by trypsinization at 80–90% confluency.

CPB2 Toxin Treatment of Cells and Total m⁶A Measurement

IPEC-J2 cells were seeded in 6-well plates at a density of 1 × 10⁵ cells/mL and cultured overnight (24 h). Then, cells in three wells were each treated with 20 μ g/mL CPB2 (treatment group) while cells in the other three wells were not exposed to toxin (control group) (Gao et al., 2020; Luo et al., 2020). Total RNA was extracted by using TRIzol reagent according to the manufacturer's instructions (Invitrogen, Carlsbad,

TABLE 1 | Primer sequences for RT-qPCR and MeRIP-qPCR.

Gene	Primer sequence (5'-3')	Product length (bp)	Accession no
<i>METTL3</i>	F: CCACTTCTGGTGGCCCTAAG R: CGCCAGATCAGAAAGTGGT	104	XM_003128580.5
<i>METTL14</i>	F: GAGATTGCAGCTCCTCGATCA R: CCCCACTTGGGTAAACACAC	89	XM_003129231.6
<i>WTAP</i>	F: GCGGGAATAAGGCCTCCAAC R: TGTGAGTGGCGTGTGAGAGA	136	XM_005659114.3
<i>FTO</i>	F: GCATGGCTGCTTATTTCCGGG R: TGCATCAGAGCCCTTCACTG	154	NM_001112692.1
<i>ALKBH5</i>	F: CCAGTTCAAGCCTATCCGGG R: ATCCACTGAGCACAGTCACG	80	XM_021067995.1
<i>YTHDF1</i>	F: ATCGCTCCTACAAGCACTC R: CTGTTTGCCTCCGATTCTGCC	111	XM_021078236.1
<i>YTHDF2</i>	F: GGACAACCTGAGCAACGAGAGA R: GCTGAGAAGTCAATCCCGCT	131	XM_005665152.3
<i>YTHDF3</i>	F: CAACCAATAGTGTGCCCCCA R: TGGGTTGGTGGAGCCTTTAC	214	XM_021089309.1
<i>YTHDC1</i>	F: TGAGAATGTGTCCCTTGCCA R: CACCTCCAGCATCTTAGCAT	230	XM_021101402.1
<i>YTHDC2</i>	F: GAAGTGATGGATGGAGCGGA R: ATATCACCACCACCTCGTGC	142	XM_021084629.1
<i>EGR1</i>	F: GGACATGGCGACAACCTTTT R: TCCCACCTAAGAGGAACCCCT	139	XM_003123974.6
<i>MYC</i>	F: TCAGAAAAAGACGTGCTGCG R: AGTTCTCCCTCCAATAGGTCA	102	NM_001005154.1
<i>FZD7</i>	F: CAAGTTCGGCTTCCAATGGC R: CATGTAGGGCGCTGTAGGAT	148	XM_013984388.2
<i>WNT9A</i>	F: GGAGAAGAAGTGCAGAGCAT R: GTATAGACCTCCTCACGCTGG	141	XM_003123611.5
<i>FOSL1</i>	F: CCCCAGTGAAGTGGTTTCAAG R: GAAGTCTCGGAACATGCCCT	137	XM_003122519.3
<i>ITGA9</i>	F: AAGACAGTTGGGACTGGGTC R: AGTGGGGCCTCCGAAAAATC	141	XM_021071659.1
<i>IL2RA</i>	F: GCAACCATGCAGCCAATCAT R: GGCTTCTTACTGCCCTTGGT	161	XM_021064060.1
<i>TLR2</i>	F: GGAGCCTTAGAAGTAGATTTG R: TGTCTCCACATTACCGAGGG	102	NM_213761.1
<i>FZD5</i>	F: TCGTGAGGCCATTACTGGGA R: TTTCGGCTTCTCAAATGCGG	94	XM_0056722133.3
<i>WNT11</i>	F: CATGCGCTTCGCTTCCACTT R: TCGGCTTCCTTTGATGTCTG	87	XM_013979149.2
<i>GAPDH</i>	F: AGTATGATTCCACCCACGGC R: TACGTAGCACCAGCATCACC	139	XM_021091114.1

United States), and the m⁶A content was detected with an m⁶A RNA methylation quantification kit (Epigentek, Farmingdale, United States). Specifically, RNA purity was confirmed according to the following ratios: A260/A280 > 1.9 and A260/A230 > 1.7. In each reaction, the RNA (200 ng) samples were treated with an m⁶A antibody, and detection was performed based on the manufacturer's instructions. Finally, the absorbance values were measured at 450 nm.

Real-Time Quantitative PCR (RT-qPCR)

RNA (800 ng) from each sample was employed to synthesize cDNA by using a reverse transcription kit (Accurate Biotechnology, Changsha, China). Thereafter, a SYBR[®] Green Premix Pro Taq HS qPCR Kit (Accurate Biotechnology) and a LightCycler 480II apparatus (Roche, Basel, Switzerland) were used to perform RT-qPCR. The sequences of the primers used in this study are presented in **Table 1**; *GAPDH* served as an

internal control. The relative levels of DEGs were determined by the 2^{-ΔΔCt} method (Livak and Schmittgen, 2001).

m⁶A-Seq and RNA-Seq Library Construction

First, RNA was extracted, and the RNA purity and integrity were analyzed. Total RNA was extracted from IPEC-J2 cells (see *CPB2 toxin treatment of cells and total m⁶A measurement*) by using TRIzol reagent (Invitrogen, Carlsbad, United States) and then quantified with a NanoDrop ND-1000 instrument (NanoDrop, Wilmington, United States). A Bioanalyzer 2100 system (Agilent, Santa Clara, United States) was used to evaluate the integrity of RNA according to the criterion of an RNA integrity number (RIN) > 7.0. RNA integrity was further confirmed by denaturing agarose gel electrophoresis. Second, the input (RNA-seq) library and the immunoprecipitation (IP) (m⁶A-seq) library were

constructed. Briefly, an Epicenter Ribo-Zero Gold Kit (Illumina, San Diego, United States) was applied to digest and remove ribosomal RNA (rRNA) from the total RNA. A Magnesium RNA Fragmentation Module (NEB, Ipswich, United States) was used to fragment the RNA into 150-nucleotide-long fragments at 86°C for 7 min. The obtained RNA fragments were then divided into two portions. One portion was used to directly construct a conventional transcriptome sequencing library, which was retained as the input RNA, while the other portion was enriched by an m⁶A-specific antibody (Synaptic Systems, Gottingen, Germany) and was retained as IP RNA. Thereafter, the IP RNA and input RNA were reverse-transcribed to cDNA by SuperScript™ II Reverse transcriptase (Invitrogen, Carlsbad, United States). The second strand of DNA was then synthesized, and adapters were added to the blunt ends of each strand (each adapter contained a T-base overhang for ligating the adapter to the A-tailed fragmented DNA) by using *E. coli* DNA polymerase I (NEB, Ipswich, United States), RNase H (NEB, Ipswich, United States) and a dUTP Solution (Thermo Fisher, San Jose, United States). Then, the two strands were digested with the enzyme UDG (NEB), after which PCR was conducted with the following program: pre-denaturation at 95°C for 3 min; eight cycles of 15 s at 98°C, 15 s at 60°C (annealing), and 30 s at 72°C (extension); and a final extension at 72°C for 5 min. The average insert size for the final cDNA library was 300 ± 50 bp. Finally, the Illumina NovaSeq™ 6000 platform (Illumina, San Diego, United States) was used to carry out double-ended sequencing according to its standard operating procedures in PE150 sequencing mode by LC Bio Technology Co., Ltd., Hangzhou, China.

Bioinformatic Analysis of m⁶A-Seq and RNA-Seq

Data quality control. We handled the raw data reads of the IP and input samples by using Fastp software (<https://github.com/OpenGene/fastp>). In this process, the reads showing adaptor contamination, presenting an N ratio >5%, and containing low-quality sequences were removed. Finally, clean reads were obtained (Chen et al., 2018; Wang et al., 2021; Zhao et al., 2021).

Peak identification and differential peak analysis. HISAT2 software (Kim et al., 2015) (<http://daehwankimlab.github.io/hisat2>) was used to map reads to the *Sus scrofa* 11.1 reference genome (ftp://ftp.ensembl.org/pub/release-96/fasta/sus_scrofa/dna/). The mapped reads of the IP and input samples were employed for differential peak analysis by using the R package exomePeak (<https://bioconductor.org/packages/exomePeak>) (Meng et al., 2014; Wang et al., 2021). The peaks were visualized with IGV software (<http://www.igv.org>) (Robinson et al., 2017; Yang et al., 2020). We annotated the peaks by using ChIPseeker (<https://bioconductor.org/packages/ChIPseeker>) (Yu et al., 2015). Finally, a motif analysis was performed with the MEME2 (<http://meme-suite.org>) (Bailey et al., 2009) and HOMER (<http://homer.ucsd.edu/homer/motif>) (Heinz et al., 2010) softwares.

DMGs and DEGs analysis. StringTie (<https://ccb.jhu.edu/software/stringtie>) was used to determine the expression levels

of all the mRNA transcripts from the input libraries by calculating their fragments per kilobase of transcript per million mapped reads (FPKM) values (total exon fragments/mapped reads [millions] × exon length [kb]) (Pertea et al., 2015), and the R package edgeR (<https://bioconductor.org/packages/edgeR>) was used to analyze the DEGs (Robinson et al., 2010). Gene Ontology (GO) and Kyoto Encyclopedia of Genes and Genomes (KEGG) analyses were performed with Database for Annotation, Visualization and Integrated Discovery by using OmicStudio tools (<https://www.omicstudio.cn/tool>) (Chen et al., 2020; Zhou et al., 2020).

m⁶A IP (MeRIP) Followed RT-qPCR (MeRIP-qPCR)

RNA (1,000 ng/μL) samples from the control and CPB2 groups (300 μL each sample) were subjected to m⁶A IP using the GenSeq® m⁶A MeRIP Kit (GenSeq Inc., Shanghai, China) according to the manufacturer's protocol (Wang et al., 2020a; Hou et al., 2021). Briefly, the RNA was fragmented into smaller pieces of 200 nt by using an RNA fragmentation reagent and then divided into 3 and 297 μL. 3 μL was directly reverse-transcribed into cDNA (input), while the 297 μL was enriched with an m⁶A antibody and then reverse-transcribed into cDNA (IP) after purification. Finally, RT-qPCR was performed for detection.

Statistical Analyses

All experimental procedures were performed at least three times. The m⁶A peaks were filtered according to two criteria: enrichment ≥2 and a *p*-value < 0.05. The differential peaks and DEGs were screened in the CPB2 group vs the control group according to a |log₂ (fold change)| >0.585 and a *p*-value < 0.05. The RT-qPCR and MeRIP-qPCR data were analyzed by using the SPSS v.21 and GraphPad Prism v.8.0 software programs. The mean ± standard deviation (SD) was used to describe the data, and statistically significant differences are denoted with one asterisk (*) for *p* < 0.05 or two asterisks (**) for *p* < 0.01.

RESULTS

Detection of Methylation-Related Enzyme Expression and m⁶A Levels

To investigate the effect of m⁶A modification in CPB2-induced IPEC-J2 cells, the mRNA expression levels of methylation-related enzymes and the total m⁶A content of the control and CPB2 groups were detected by RT-qPCR and with an m⁶A RNA methylation quantification kit, respectively. As shown in **Figures 1A,B**, the expression levels of *METTL3*, *ALKBH5*, and *YTHDF3* were increased dramatically (*p* < 0.01), while those of *METTL14*, *FTO*, and *YTHDC2* were decreased significantly in the CPB2 toxin group relative to the control group (*p* < 0.01); *WTAP* and *YTHDC1* levels were also decreased (*p* < 0.05), but *YTHDF1* and *YTHDF2* levels were not changed (*p* > 0.05) (**Figure 1A**). In addition, the total m⁶A level was obviously increased in the CPB2 group (*p* < 0.01, **Figure 1B**). These results suggested that

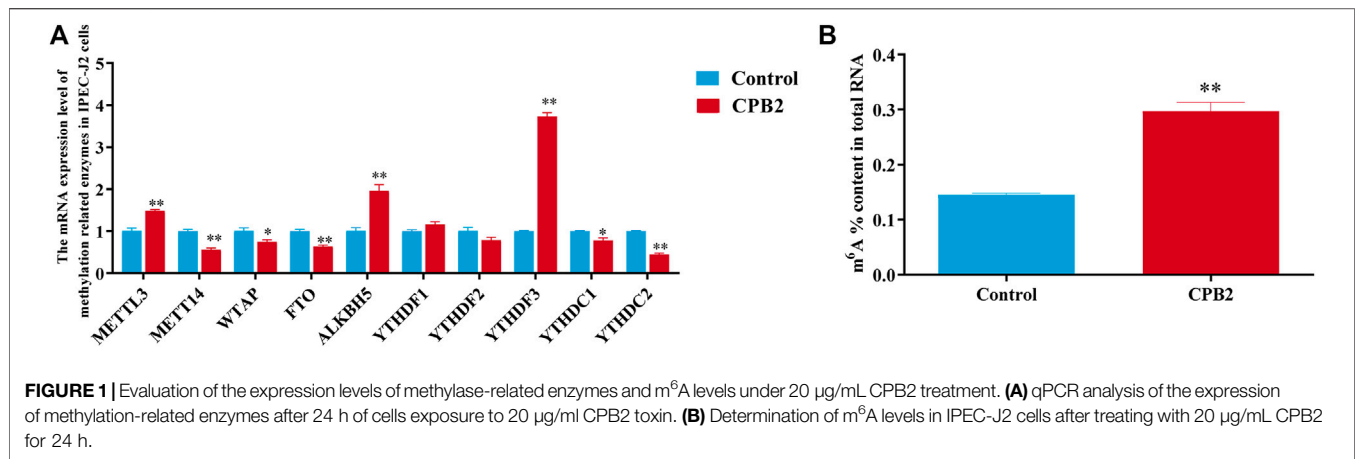


TABLE 2 | Sequence statistics and quality control.

Sample ID	Raw reads	Valid reads	Valid%	Q20%	Q30%	GC%
Control1_IP	85,492,316	82,300,032	87.19	96.52	90.94	52.87
Control2_IP	87,774,992	84,673,108	88.09	96.52	90.97	53.28
Control3_IP	86,612,186	83,480,924	87.76	96.33	90.59	53.39
CPB2_1_IP	90,242,216	86,944,982	87.8	96.56	91.01	52.96
CPB2_2_IP	86,934,932	83,429,868	86.82	96.39	90.78	53.41
CPB2_3_IP	89,642,446	86,070,422	86.79	96.41	90.77	53.99
Control1_input	97,586,308	93,048,292	84.9	96.54	91.09	55.12
Control2_input	96,994,146	92,000,280	84.62	96.53	91.09	55.3
Control3_input	93,495,320	88,512,112	84.2	96.3	90.67	55.92
CPB2_1_input	95,043,768	90,159,134	84.15	96.58	91.17	55.18
CPB2_2_input	97,478,686	91,769,152	83.24	96.37	90.85	55.73
CPB2_3_input	92,752,804	88,474,096	84.76	96.46	90.95	55.71

differences in m⁶A methylation modifications may exist between the control group and the CPB2 group.

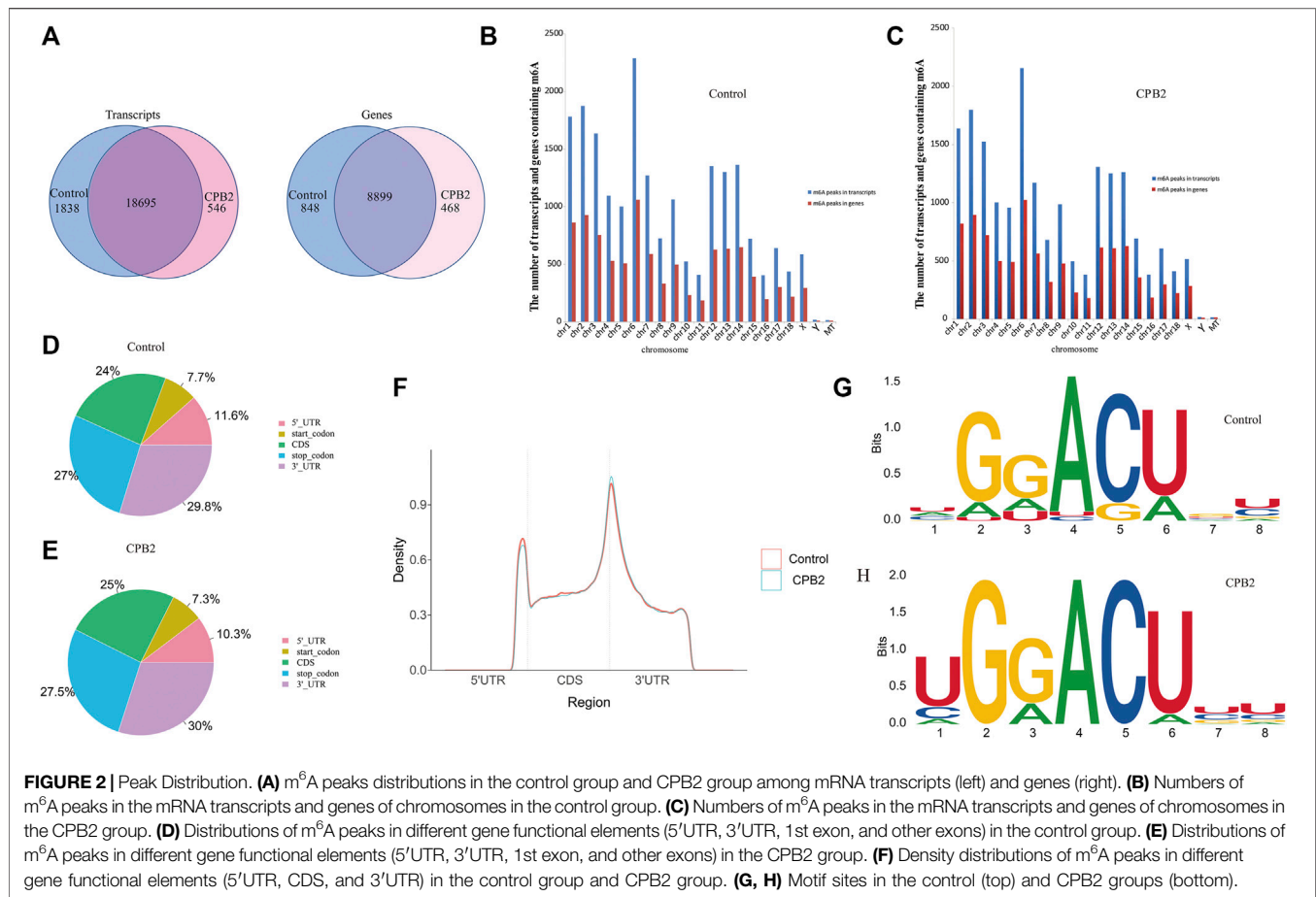
Sequence Statistics and Quality Control

To further explore the biological process of m⁶A modification in IPEC-J2 cells exposed to CPB2 toxin, three samples each from the control and CPB2 groups were collected for m⁶A sequencing. Two types of libraries corresponding to the control group and CPB2 group were further constructed and designated the IP libraries (m⁶A-seq) and the input libraries (RNA-seq), respectively. For the IP libraries, a total of 89,642,446–90,242,216 raw reads were obtained for the CPB2 group, while 85,492,316–87,774,992 raw reads were obtained for the control group (Table 2). For the input libraries, there were 92,752,804–97,478,686 raw reads for the CPB2 group and 93,495,320–97,586,308 raw reads for the control group (Table 2). The percentages of clean (valid) reads for the control group and the CPB2 group were greater than 86.79% in the IP libraries and 83.24% in the input libraries. For all libraries, the Q20 and Q30 values were at least 90% (Table 2 and Supplementary Table S1). In addition, clean reads whose ribosome sequences were removed were compared with the porcine reference genome. The results showed that the clean reads were mainly aligned to exon regions, introns, and intergenic regions, and the proportions

of exons exceeded 60% in the control and CPB2 groups (Supplementary Figure S1; Table S2).

Peak Distributions of m⁶A Modifications in the Whole Genome

After the full-range peak calling results of the porcine reference genome were scanned, a Poisson distribution model was used to check the reads of the candidate peak regions and to calculate the *p*-values of given peak regions. In this experiment, we were able to distinguish the differences in these peaks (i.e., enrichment ≥2, *p* < 0.05) and identify the peaks in the IP libraries, whose results were compared with those of the input libraries. We found that the numbers of peaks in the control group vs the CPB2 group were 20,533 and 19,241, respectively (Supplementary Table S3). Additionally, 18,695 peaks were the same between the control group and the CPB2 group, accounting for 90% of all detected peaks (Figure 2A). Furthermore, we analyzed the distributions of peaks on the pig chromosomes in the CPB2 group and control group. Interestingly, there were more peaks on chromosomes 1, 2, 3, 6, 12, 13, and 14 than on other chromosomes, and the most peaks were distributed on chromosome 6 (Figures 2B,C, Supplementary Table S4). Then, we analyzed the distributions of peaks in gene functional elements in both groups. The results showed that the m⁶A peaks in the control



group and CPB2 group were mainly enriched in the 3'UTRs and stop codon regions (Figures 2D,E, Figure 2F). Next, HOMER and MEME2 softwares were employed to identify the most reliable motifs in the peak regions, which identified the GGACU motif in the control group and the UGGACU motif in the CPB2 group (Figures 2G,H).

Differential m⁶A Peaks Between the CPB2 and Control Groups

To analyze the distributions of m⁶A peaks among the different chromosomes, genes, and mRNA transcripts in the CPB2 and control groups, we scanned the differential peaks and found 1,448 differential m⁶A peaks. Among these peaks, we found 437 significantly upregulated peaks in 394 genes (here referred to as differentially methylated genes, DMGs) and 1,011 significantly downregulated peaks in 920 genes (Figure 3A and Supplementary Table S5). The top 20 altered m⁶A peaks represented the 10 most upregulated genes and the 10 most downregulated genes (Table 3 and Supplementary Table S5). Furthermore, relative to the control group (excluding the peaks showing no significant difference on the mitochondrial chromosome), the CPB2 group exhibited differential peaks distributed on other chromosomes; there were more downregulated peaks than upregulated peaks, and the peaks

were most abundant on chromosome 6 (Figure 3B and Supplementary Table S6). We also counted the peaks distributed in genes and found that many genes contained one peak, which accounted for 46.7% (184/394) of the DMGs with upregulated peaks and 48.9% (452/920) DMGs with downregulated (Figure 3C and Supplementary Table S7). In analyzing the number of differential peaks among all mRNA transcripts, we found that the majority of mRNA transcripts in the whole genome showed one peak, while a few mRNA transcripts showed two or more differential peaks (Figure 3D and Supplementary Table S7). In addition, we calculated the densities of m⁶A modifications among mRNA molecules and found that the gene fragments containing more m⁶A peaks were longer (Figure 3E).

GO and KEGG Analysis of Genes Presenting Differential m⁶A Peaks (DMGs)

To investigate the biological processes associated with m⁶A modification in IPEC-J2 cells in response to CPB2 infection, we analyzed the functions of DMGs presenting upregulated m⁶A peaks (n = 437) or downregulated peaks (n = 1,011) according to GO terms and KEGG signaling pathways. The GO results were divided into three categories: the biological process (BP), cellular component (CC), and molecular function (MF) categories. The

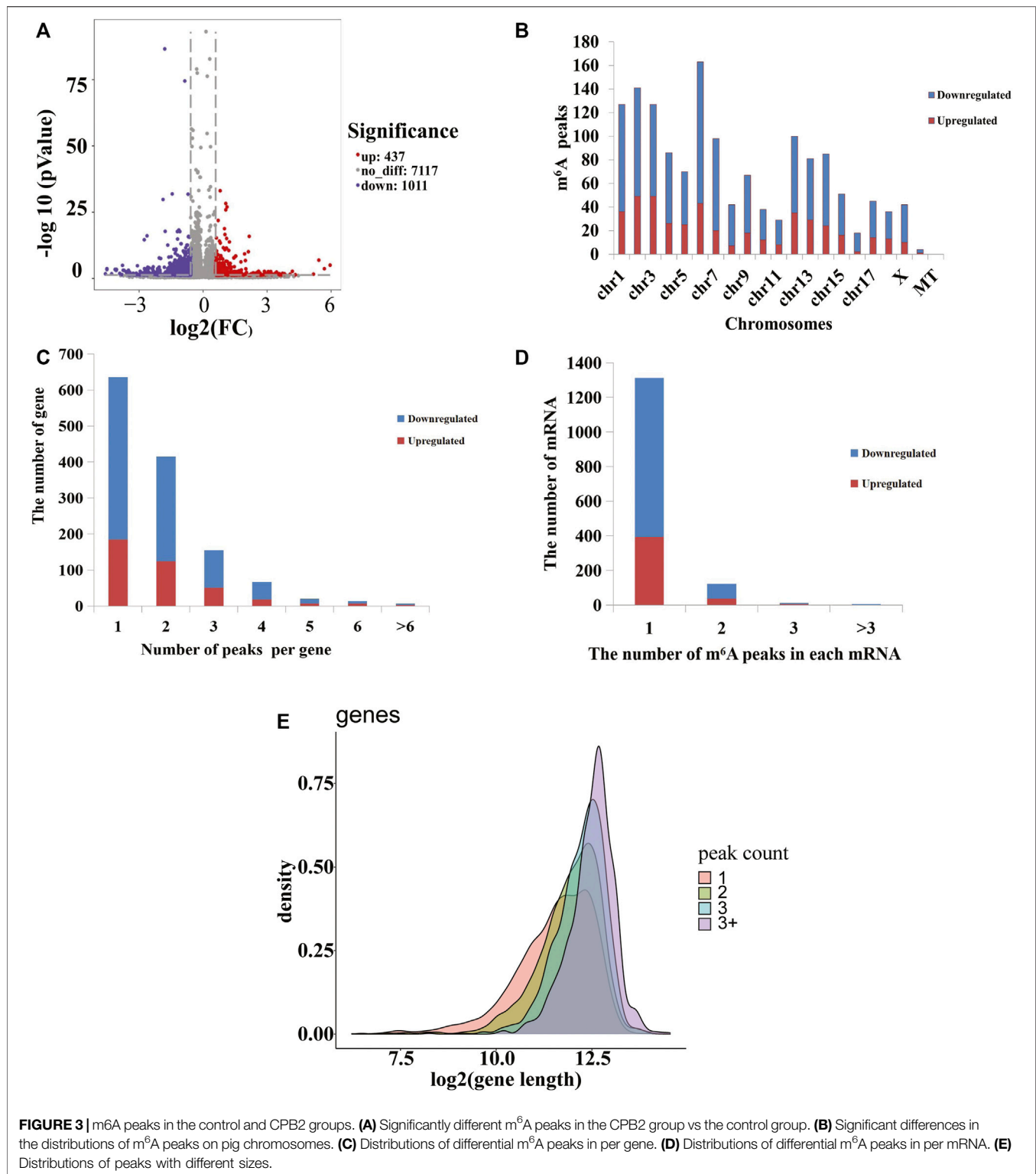


FIGURE 3 | m⁶A peaks in the control and CPB2 groups. **(A)** Significantly different m⁶A peaks in the CPB2 group vs the control group. **(B)** Significant differences in the distributions of m⁶A peaks on pig chromosomes. **(C)** Distributions of differential m⁶A peaks in per gene. **(D)** Distributions of differential m⁶A peaks in per mRNA. **(E)** Distributions of peaks with different sizes.

top 10 BP, CC, and MF terms that were enriched for genes with upregulated and downregulated m⁶A peaks are shown in **Figures 4A,B**. For the KEGG pathway analysis, we display the top 10 enriched KEGG pathways based on their *p*-values. The results showed that genes with upregulated m⁶A peaks were mainly

enriched in cancer signaling pathways (20 genes), the Cushing syndrome signaling pathway (9 genes), and the Wnt signaling pathway (9 genes) (**Figure 4C** and **Supplementary Table S5**), while genes with downregulated m⁶A peaks were mainly enriched in the apoptosis pathway (15 genes), the small cell lung cancer

TABLE 3 | Top 10 significantly upregulated and top 10 significantly downregulated m⁶A peaks (CPB2 vs control).

Chromosome	Peak start	Peak end	Gene ID	Gene name	Regulation	p-value	Log2 (fold change)	Peak region
chr12	41,074,651	41,075,895	ENSSSCG00000031620	ENSSSCG00000031620	up	8.91E-06	5.95	3'UTR
chr3	10,755,262	10,755,381	ENSSSCG00000023004	FZD9	up	0.00020417	5.68	CDS
chr18	6,382,439	6,383,066	ENSSSCG00000033909	ENSSSCG00000033909	up	1.20E-07	5.42	CDS
chr9	121,457,341	121,457,431	ENSSSCG00000033352	FAM163A	up	0.02238721	5.17	3'UTR
chr10	28,509,561	28,509,920	ENSSSCG00000033321	GAS1	up	0.03890451	4.32	CDS
chr15	140,319,882	140,320,272	ENSSSCG00000034101	D2HGDH	up	0.00194984	4.18	CDS
chr2	70,622,697	70,622,965	ENSSSCG00000013607	ENSSSCG00000013607	up	0.02570396	4.07	5'UTR
chr3	113,558,282	113,558,342	ENSSSCG00000029413	DNMT3A	up	0.01659587	3.81	CDS
chr4	98,093,837	98,093,896	ENSSSCG00000006634	TNFAIP8L2	up	0.03311311	3.81	3'UTR
chr8	12,807,001	12,807,091	ENSSSCG00000008747	NCAPG	up	0.01202264	3.72	3'UTR
chrY	25,251,102	25,252,331	ENSSSCG00000034853	ENSSSCG00000034853	down	0	-10.1	3'UTR
chr6	54,469,817	54,469,877	ENSSSCG00000038579	DKKL1	down	0.01737801	-4.58	3'UTR
chr4	97,240,279	97,240,459	ENSSSCG00000006610	S100A11	down	0.00019953	-4.51	3'UTR
chr7	52,922,051	52,922,196	ENSSSCG00000035897	ENSSSCG00000035897	down	0.00041687	-4.51	CDS
chr7	23,655,139	23,655,378	ENSSSCG00000014000	DDX39B	down	0.01659587	-4.29	3'UTR
chr7	36,352,159	36,352,488	ENSSSCG00000038553	TSPO2	down	0.00038905	-4.13	3'UTR
chr4	99,142,708	99,142,917	ENSSSCG00000006666	SV2A	down	0.00091201	-4.08	5'UTR
chrX	58,487,996	58,488,554	ENSSSCG00000011830	ENSSSCG00000011830	down	0.00039811	-4.06	CDS
chrY	25,253,141	25,253,380	ENSSSCG00000034853	ENSSSCG00000034853	down	0.01230269	-3.91	3'UTR
chr6	159,511,892	159,511,981	ENSSSCG00000027119	SELRC1	down	0.03311311	-3.81	5'UTR

signaling pathway (11 genes) and the herpes simplex virus 1 infection signaling pathway (27 genes) (Figure 4D and Supplementary Table S5).

DEGs (RNA-Seq Data) Following CPB2 Treatment of IPEC-J2 Cells

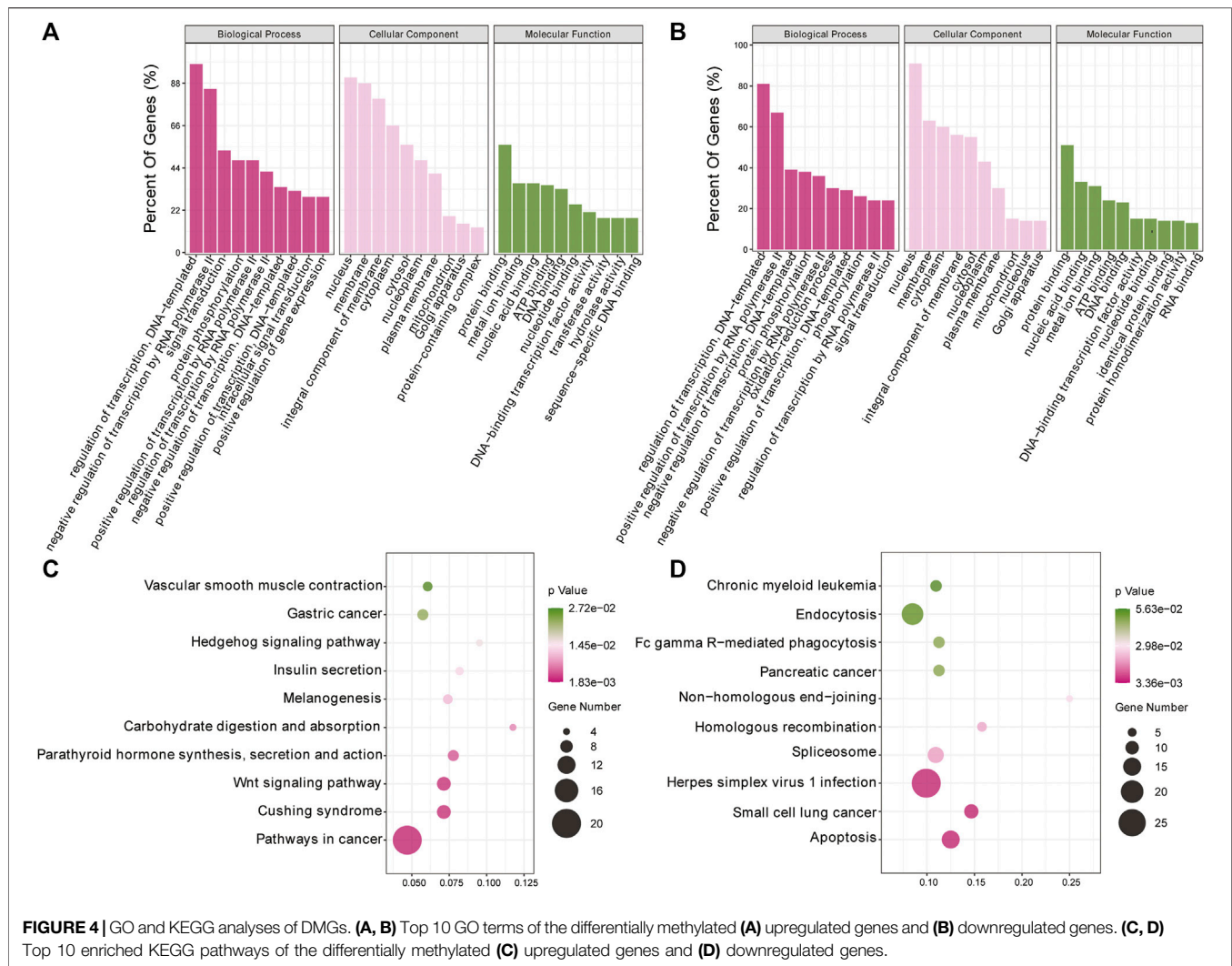
We used RNA-seq data (the m⁶A-seq input library) to analyze DEGs after treating IPEC-J2 cells with CPB2 (Figures 5A,B, Supplementary Table S8). In total, 1,636 DEGs were detected in the CPB2 group relative to the control group, among which 1,094 DEGs were upregulated and 542 DEGs were downregulated. We list the top 20 most significantly upregulated genes and downregulated genes in tables (10 of each; Table 4, Supplementary Table S8), and the top 10 GO terms and top 10 KEGG pathways of the DEGs are displayed in Figure 5C, Figure 5D, and Supplementary Table S8. Both upregulated and downregulated genes were involved in the regulation of transcription, DNA templates, and signal transduction as well as the positive regulation of transcription by RNA polymerase in the BP category. The upregulated genes also participated in immune and inflammatory responses. The KEGG results indicated that upregulated genes were enriched predominantly in pathways related to influenza A cytokine-cytokine receptor interaction, cell adhesion molecules (CAMs), *Staphylococcus aureus* infection, NOD-like receptors, chemokines and TNF signaling pathways. The downregulated genes were involved in pathways related to Hippo signaling, Wnt signaling, terpenoid backbone biosynthesis, proteoglycans in cancer, melanogenesis, bladder cancer, transcriptional misregulation in cancer, basal cell carcinoma, glycolysis/gluconeogenesis, and TGF-beta signaling.

Combined m⁶A-Seq and RNA-Seq Analysis

To further explore the functional significance of m⁶A modification in IPEC-J2 cells in response to CPB2, we investigated whether m⁶A methylation was the basis of the observed expression differences. For this purpose, m⁶A-seq data and RNA-seq data were used to detect DMGs and DEGs. Thereafter, combined m⁶A-seq and RNA-seq analysis divided a total of 192 genes into four main groups (Figure 6A and Supplementary Table S9): a group of 52 hypermethylated and upregulated genes (hyper-up genes), a group of 47 hypomethylated and downregulated genes (hypo-down genes), a group of 18 hypermethylated and downregulated genes (hyper-down genes) and a group of 75 hypomethylated and upregulated genes (hypo-up genes). The 18 hyper-down genes, 52 hyper-up genes and 75 hypo-up genes were further investigated by KEGG analysis, which revealed that the top 10 enriched KEGG pathways among the hyper-down genes were mainly related to glycolysis/gluconeogenesis; neomycin, kanamycin, gentamicin biosynthesis and Wnt signaling pathways (Figure 6B and Supplementary Table S9). In contrast, the hyper-up genes were mainly enriched in the CAMs signaling pathway (Figure 6C and Supplementary Table S9). In addition, the 75 hypo-up genes were mainly enriched in signaling pathways such as the FoxO, Hippo, and basal cell carcinoma pathways (Figure 6D and Supplementary Table S9).

Validation of DEGs and DMGs by qPCR and MeRIP-qPCR

To verify the m⁶A-seq and RNA-seq data, we randomly selected 10 DEGs (*EGRI*, *MYC*, *FZD7*, *WNT9A*, *FOSL1*, *ITGA9*, *IL2RA*, *TLR2*, *FZD5*, and *WNT11*) and checked the reliability of the RNA-seq data by RT-qPCR. According to the combined m⁶A-seq

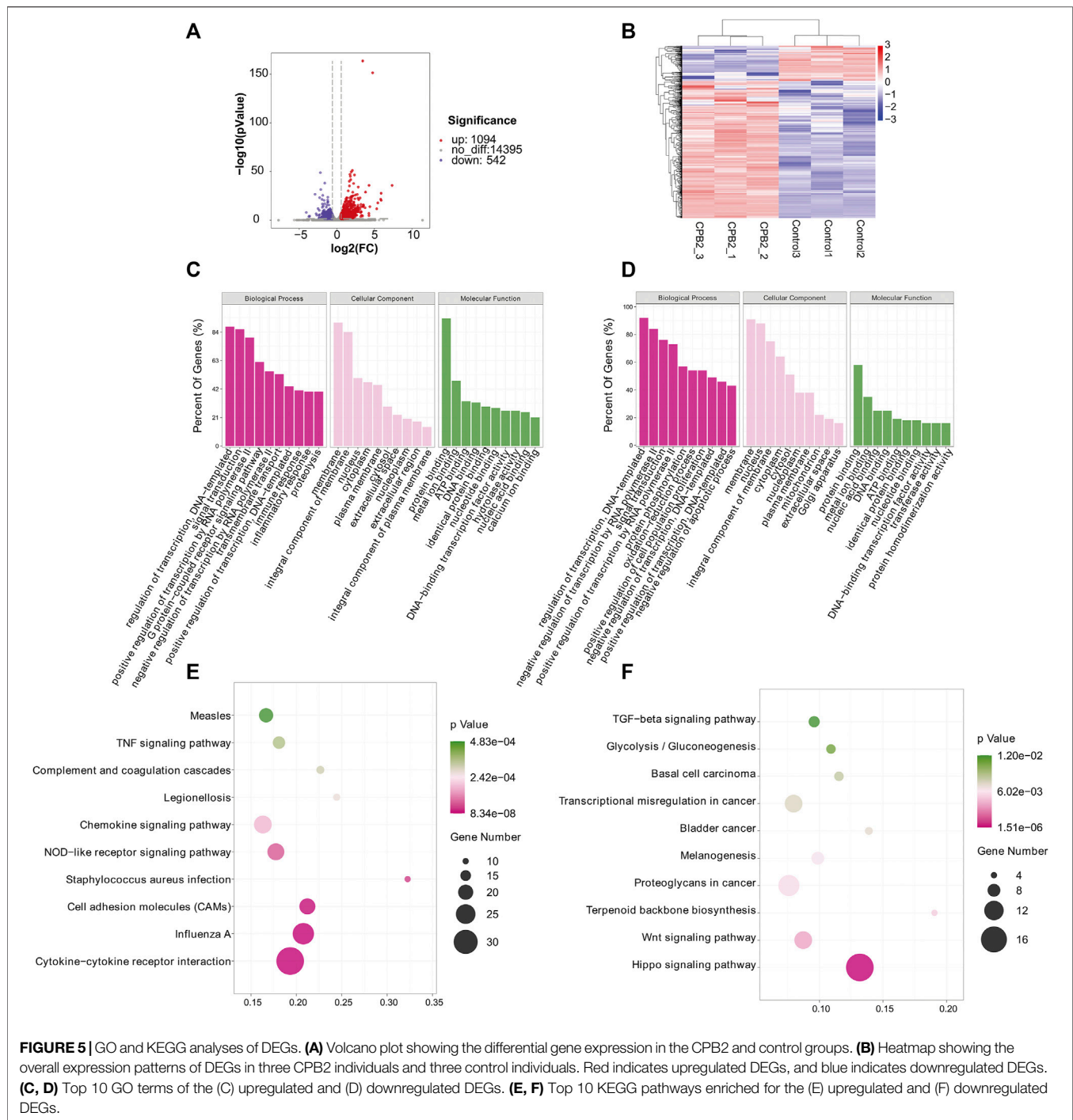


and RNA-seq analysis results, three DMGs (*WNT9A*, *FOSL1*, and *WNT11*) were selected for the MeRIP-qPCR assay. The RT-qPCR and MeRIP-qPCR results (**Figures 7A,B**) were consistent with the RNA-seq and m⁶A-seq results, thus confirming the reliability of the results of our m⁶A-seq experiment.

DISCUSSION

Similar to DNA and protein modifications, m⁶A modification is a dynamically reversible posttranscriptional change that mainly regulates mRNA expression, splicing, structure, stability, lifespan, and degradation as well as RNA modification during translation (Fu et al., 2014; Adhikari et al., 2016). This modification plays roles in bacterial and viral infections, intestinal diseases, and host immune responses (Sebastian-delacruz et al., 2020; Wu et al., 2020). Feng et al. (2018) demonstrated that the expression levels of m⁶A and *METTL3* were upregulated in HDPCs stimulated by LPS. Similarly, in another study, both the m⁶A levels and the mRNA expression of

WTAP increased when THP-1 cells were treated with heat-killed *Salmonella typhimurium* (HKST) (Wu et al., 2020). However, Zong et al. found that when IPEC-J2 cells were infected with *E. coli* K88, the methylation level of m⁶A was significantly reduced, while the expression of m⁶A reader proteins (*YTHDF1* and *YTHDF2*) were markedly increased, and the expression of the methyltransferase *METTL3* and the demethylase *FTO* were not changed; moreover, *E. coli* K88 infection was shown to cause intestinal inflammation and to impair lipid transport in the *YTHDF1*-dependent m⁶A pathway in IPEC-J2 cells (Zong et al., 2018). In this experiment, we detected the mRNA expression of methylation-related enzymes and the overall level of m⁶A methylation, and the results demonstrated that the mRNA expression levels of the methyltransferases *METTL3*, *METTL14*, and *WTAP* and the demethylases *FTO* and *ALKBH5* were altered, while the overall m⁶A level was increased significantly. Therefore, we speculate that the m⁶A methylation modification may be involved in the CPB2-induced inflammatory response of IPEC-J2 cells.

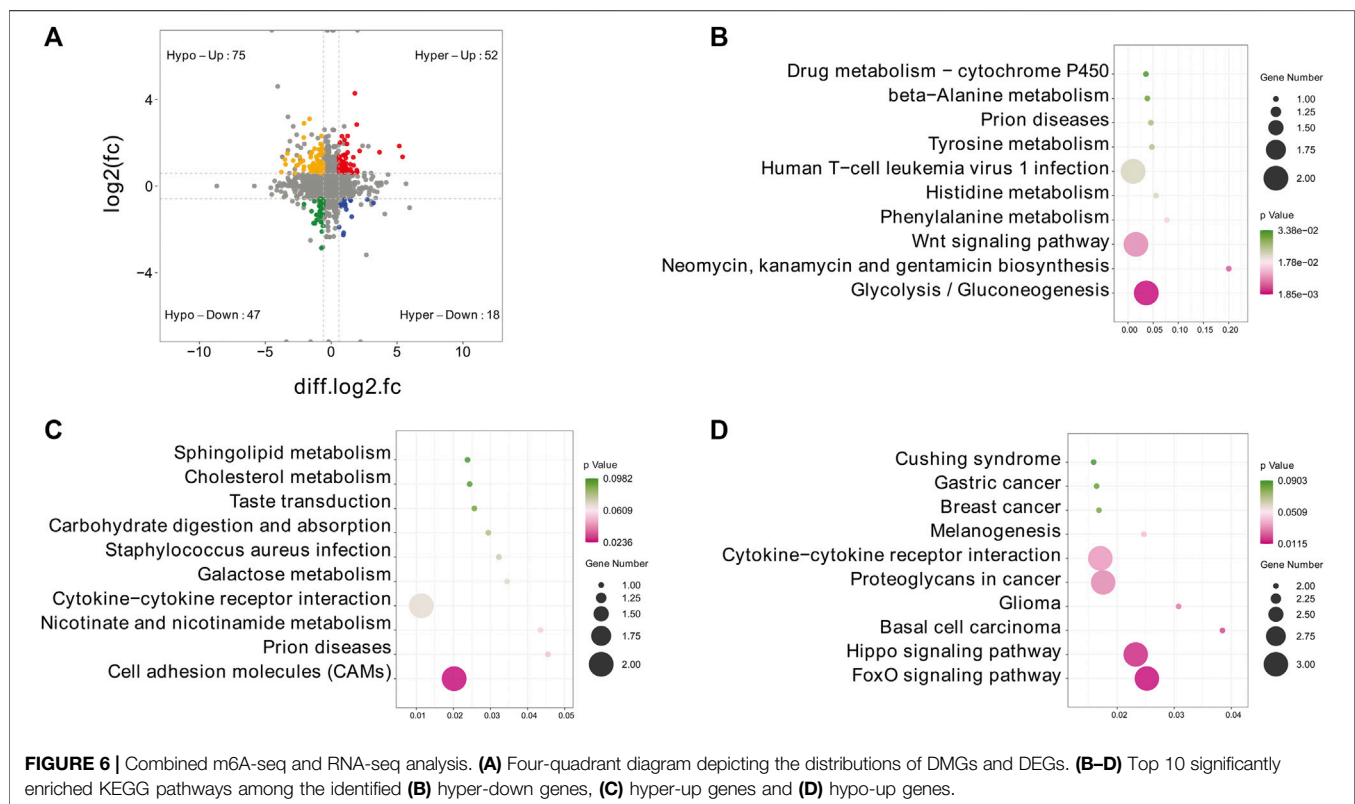


In this study, we found 18,695 peaks that were the same in the CPB2 and control groups, which accounted for 90% of all the peaks. This indicated that most of the peaks corresponded to functions that maintained the physiological homeostasis of the organism. In mouse tissues and human cells, m⁶A has been shown to be located mainly near stop codons and 3'UTRs (Dominissini et al., 2012; Meyer et al., 2012). We analyzed the distributions of m⁶A peaks in different gene functional elements and found that m⁶A peaks were indeed mainly distributed in

3'UTRs and stop codon regions. These findings are consistent with those of Wang et al. (2020b) and prove that m⁶A motif enrichment is more common in 3'UTRs than in other regions. The 3'UTR regulates the stability, localization, expression, and translation of mRNA. Multiple RNA-binding proteins bind in this region to perform regulatory functions and regulate protein-protein interactions (Mayr, 2018). The m⁶A methylation recognition proteins, YTHDF1 and YTHDF2, mainly recognize the m⁶A motifs of 3'UTRs and alter the

TABLE 4 | Top 10 upregulated and top 10 downregulated DEGs (CPB2 vs control).

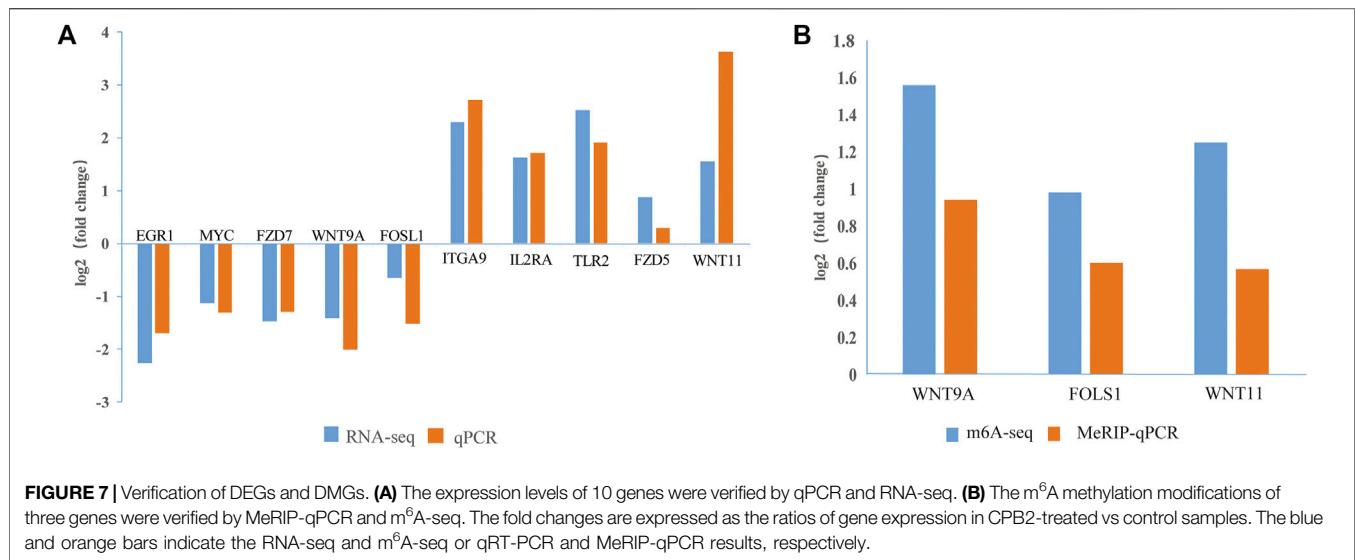
Gene name	Locus	Regulation	Fold change	p-value
OLFM4	chr11:26,350,032–26,375,740	up	164.4964353	1.90719E-36
CCL17	chr6:19,345,764–19,348,965	up	60.09315203	4.09127E-21
HHATL	chr13:26,205,616–26,219,937	up	59.85677737	1.96714E-28
GC	chr8:68,326,287–68,364,937	up	57.73376422	3.20932E-22
PRICKLE2	chr13:45,620,368–45,789,113	up	43.95440161	1.42386E-18
C3	chr2:72,431,163–72,471,564	up	27.30318327	3.2955E-152
SLFN11	chr12:39,986,366–39,992,685	up	21.62979927	1.75657E-14
ADORA2A	chr14:49,468,862–49,487,628	up	14.17608216	1.33747E-29
PCP4L1	chr4:89,186,937–89,212,840	up	13.8161881	2.28515E-13
CCL22	chr6:19,296,637–19,302,737	up	11.84724721	1.74685E-16
ZSCAN26	chrX:45,772,497–45,798,482	down	0.137483812	3.34197E-27
ZFAND1	chr15:32,408,854–32,475,979	down	0.151873654	2.66575E-07
ITGA1	chr6:47,643,560–47,657,784	down	0.161195423	9.01136E-06
OCA2	chr7:22,114,800–22,133,148	down	0.18087438	1.64436E-12
NAB2	chr4:54,908,876–54,931,825	down	0.195968666	1.13013E-05
ZMAT2	chr16:32,185,484–32,295,491	down	0.19937155	0.012466794
ANKRD61	chr15:56,657,598–56,869,920	down	0.199594035	0.003131712
SPRY4	chr5:22,400,548–22,410,479	down	0.203847311	1.0527E-10
EGR1	chr2:142,411,086–142,417,154	down	0.209337433	9.52077E-24
MFAP3	chr3:5,097,791–5,117,889	down	0.210674837	3.27485E-06



translation efficiency and degradation rate of m⁶A-modified RNA (Wang et al., 2015; Chen et al., 2018). A conserved m⁶A motif sequence, gg (R: G, A, U; R: G, A; H: U, A, C), was recently reported (Han et al., 2019). Our results revealed conserved m⁶A motifs of GGACU and UGGACU in the control and CPB2 groups, respectively, similar to the findings of Han et al.

(2019). These results suggest that these motifs may be recognized by certain proteins and play important roles in IPEC-J2 cells in response to CPB2.

Relative to the control group, the CPB2 group exhibited 1,448 differential peaks (437 upregulated and 1,011 downregulated). The DMGs with upregulated peaks were mainly enriched in cancer



signaling pathways, the Cushing syndrome signaling pathway and the Wnt signaling pathway. Interestingly, some of these genes appeared simultaneously in many signaling pathways. For example, *WNT11*, *WNT9A*, and *FZD9* were all enriched in cancer signaling pathways, the Cushing syndrome signaling pathway, and the Wnt signaling pathway. These three genes encode the main ligands and receptors that regulate the activation and deactivation of the Wnt signaling pathway. The Wnt signaling pathway impacts intestinal balance, self-renewal, and malignant transformation (Liu et al., 2011). The *WNT11* gene is a novel important contributor to intestinal homeostasis and host defense and participates in the protection of host intestinal cells by blocking the invasion of pathogenic bacteria, inhibiting inflammation, and inhibiting apoptosis (Liu et al., 2011). In addition, some studies have indicated that *WNT11* regulates the development of the heart and kidneys via an atypical Wnt signaling pathway and inhibits the inflammation of intestinal epithelial cells (Pandur et al., 2002; Majumdar et al., 2003; Liu et al., 2011). *WNT9A* is considered to act as a tumor suppressor gene in relation to the development of colorectal cancer (Ali et al., 2016). Intriguingly, according to the GO and KEGG analyses, we found that the DMGs and DEGs were almost always significantly enriched in the Wnt signaling pathway. Therefore, we propose that m⁶A modification is involved in the inflammatory response induced by CPB2 in IPEC-J2 cells and that it may modulate this inflammatory response by influencing the gene expression of the Wnt signaling pathway.

CONCLUSION

In this study, we analyzed how m⁶A methylation is modified in CPB2-induced IPEC-J2 cells. The results suggest that m⁶A methylation may play a role in the Wnt signaling pathway in CPB2-induced IPEC-J2 cells and exert anti-inflammatory or proinflammatory effects on intestinal diseases. These findings provide a basis for further research into the functions of m⁶A methylation modifications in CPB2 toxin-induced piglet diarrhea.

DATA AVAILABILITY STATEMENT

Our data are deposited in the G E O repository, the accession number: GSE167267. We have published our data on October 5, 2021. The link for data disclosure is as follows: <https://www.ncbi.nlm.nih.gov/geo/query/acc.cgi?acc=GSE167267>.

AUTHOR CONTRIBUTIONS

JZ, QY, ZY, and SG conceived the project; JZ, JY, RL, XG, XH, and PW designed most experiments; WW, KX, XG, RL, and BZ performed data analyses; JZ, JY, WW, KX, RL and XG performed the experiments; and JZ wrote the paper with suggestions from SG.

FUNDING

This work was supported by Education Science and Technology Innovation Project of Gansu Province (GSSYLXM-02), the National Natural Science Foundation of China (31960646), the Youth Science and Technology Fund Program of Gansu Province (20JR5RA005) and the Education Department of Gansu Province: Excellent Graduate student “Innovation Star” project 2021CXZX-351.

ACKNOWLEDGMENTS

We thank LC-BIO Biotech Ltd. (Hangzhou, China) for supporting the high-throughput sequencing instrument.

SUPPLEMENTARY MATERIAL

The Supplementary Material for this article can be found online at: <https://www.frontiersin.org/articles/10.3389/fgene.2021.689748/full#supplementary-material>.

REFERENCES

- Adhikari, S., Xiao, W., Zhao, Y.-L., and Yang, Y.-G. (2016). m⁶A: Signaling for mRNA Splicing. *RNA Biol.* 13 (9), 756–759. doi:10.1080/15476286.2016.1201628
- Alarcón, C. R., Goodarzi, H., Lee, H., Liu, X., Tavazoie, S., and Tavazoie, S. F. (2015). HNRNPA2B1 Is a Mediator of m⁶A-dependent Nuclear RNA Processing Events. *Cell* 162 (6), 1299–1308. doi:10.1016/j.cell.2015.08.011
- Ali, I., Medegan, B., and Braun, D. (2016). WNT9A Induction Linked to Suppression of Human Colorectal Cancer Cell Proliferation. *Ijms* 17 (4), 495–506. doi:10.3390/ijms17040495
- Bailey, T. L., Boden, M., Buske, F. A., Frith, M., Grant, C. E., Clementi, L., et al. (2009). MEME SUITE: Tools for Motif Discovery and Searching. *Nucleic Acids Res.* 37, W202–W208. doi:10.1093/nar/gkp335
- Chen, J., Zhang, Z., Lei, Z., Shimizu, K., Yao, P., Su, Z., et al. (2020). Occurrence and Distribution of Antibiotic Resistance Genes in the Coastal Sediments of Effluent-Receiving Areas of WWTPs, China. *Bioresour. Tech. Rep.* 11 (100511), 100511–100517. doi:10.1016/j.biteb.2020.100511
- Chen, S., Zhou, Y., Chen, Y., and Gu, J. (2018). Fastp: an Ultra-fast All-In-One FASTQ Preprocessor. *Bioinformatics* 34 (17), i884–i890. doi:10.1093/bioinformatics/bty560
- Dominissini, D., Moshitch-Moshkovitz, S., Schwartz, S., Salmon-Divon, M., Ungar, L., Osenberg, S., et al. (2012). Topology of the Human and Mouse m⁶A RNA Methylomes Revealed by m⁶A-Seq. *Nature* 485 (7397), 201–206. doi:10.1038/nature11112
- Feng, Z., Li, Q., Meng, R., Yi, B., and Xu, Q. (2018). METTL3 Regulates Alternative Splicing of MyD88 upon the Lipopolysaccharide-induced Inflammatory Response in Human Dental Pulp Cells. *J. Cel. Mol. Med.* 22 (5), 2558–2568. doi:10.1111/jcmm.13491
- Fu, Y., Dominissini, D., Rechavi, G., and He, C. (2014). Gene Expression Regulation Mediated through Reversible m⁶A RNA Methylation. *Nat. Rev. Genet.* 15 (5), 293–306. doi:10.1038/nrg3724
- Fustin, J.-M., Doi, M., Yamaguchi, Y., Hida, H., Nishimura, S., Yoshida, M., et al. (2013). RNA-methylation-dependent RNA Processing Controls the Speed of the Circadian Clock. *Cell* 155, 793–806. doi:10.1016/j.cell.2013.10.026
- Gao, X., Yang, Q., Huang, X., Yan, Z., Zhang, S., Luo, R., et al. (2020). Effects of *Clostridium perfringens* Beta2 Toxin on Apoptosis, Inflammation, and Barrier Function of Intestinal Porcine Epithelial Cells. *Microb. Pathogenesis* 147, 104379. doi:10.1016/j.micpath.2020.104379
- Garcia, J. P., Beingsser, J., Fisher, D. J., Sayeed, S., McClane, B. A., Posthaus, H., et al. (2012). The Effect of *Clostridium perfringens* Type C Strain CN3685 and its Isogenic Beta Toxin Null Mutant in Goats. *Vet. Microbiol.* 157 (3–4), 412–419. doi:10.1016/j.vetmic.2012.01.005
- Gibert, M., Jolivet-Renaud, C., and Popoff, M. R. (1997). Beta2 Toxin, a Novel Toxin Produced by *Clostridium perfringens*. *Gene* 203 (1), 65–73. doi:10.1016/s0378-1119(97)00493-9
- Han, D., Liu, J., Chen, C., Dong, L., Liu, Y., Chang, R., et al. (2019). Anti-tumour Immunity Controlled through mRNA m⁶A Methylation and YTHDF1 in Dendritic Cells. *Nature* 566 (7743), 270–274. doi:10.1038/s41586-019-0916-x
- Heinz, S., Benner, C., Spann, N., Bertolino, E., Lin, Y. C., Laslo, P., et al. (2010). Simple Combinations of Lineage-Determining Transcription Factors Prime Cis-Regulatory Elements Required for Macrophage and B Cell Identities. *Mol. Cell* 38, 576–589. doi:10.1016/j.molcel.2010.05.004
- Hou, G., Zhao, X., Li, L., Yang, Q., Liu, X., Huang, C., et al. (2021). SUMOylation of YTHDF2 Promotes mRNA Degradation and Cancer Progression by Increasing its Binding Affinity with m⁶A-Modified mRNAs. *Nucleic Acids Res.* 49 (5), 2859–2877. doi:10.1093/nar/gkab065
- Huang, H., Weng, H., and Chen, J. (2020). m⁶A Modification in Coding and Non-coding RNAs: Roles and Therapeutic Implications in Cancer. *Cancer Cell* 37 (3), 270–288. doi:10.1016/j.ccell.2020.02.004
- Huang, H., Weng, H., Sun, W., Qin, X., Shi, H., Wu, H., et al. (2018). Recognition of RNA N⁶-Methyladenosine by IGF2BP Proteins Enhances mRNA Stability and Translation. *Nat. Cel Biol* 20 (3), 285–295. doi:10.1038/s41556-018-0045-z
- Immerseel, F. V., Buck, J. D., Pasmans, F., Huyghebaert, G., Haesebrouck, F., and Ducatelle, R. (2004). *Clostridium Perfringens* Poultry: an Emerging Threat for Animal and Public Health. *Avian Pathol.* 33 (6), 537–549. doi:10.1080/03079450400013162
- Kim, D., Langmead, B., and Salzberg, S. L. (2015). HISAT: a Fast Spliced Aligner with Low Memory Requirements. *Nat. Methods* 12 (4), 357–360. doi:10.1038/nmeth.3317
- Liu, N., Dai, Q., Zheng, G., He, C., Parisien, M., and Pan, T. (2015). N⁶-methyladenosine-dependent RNA Structural Switches Regulate RNA-Protein Interactions. *Nature* 518 (7540), 560–564. doi:10.1038/nature14234
- Liu, X., Wu, S., Xia, Y., Li, X. E., Xia, Y., Zhou, Z. D., et al. (2011). Wingless Homolog Wnt11 Suppresses Bacterial Invasion and Inflammation in Intestinal Epithelial Cells. *Am. J. Physiology-Gastrointestinal Liver Physiol.* 301 (6), G992–G1003. doi:10.1152/ajpgi.00080.2011
- Livak, K. J., and Schmittgen, T. D. (2001). Analysis of Relative Gene Expression Data Using Real-Time Quantitative PCR and the 2⁻ΔΔCT Method. *Methods* 25 (4), 402–408. doi:10.1006/meth.2001.1262
- Luo, R., Yang, Q., Huang, X., Yan, Z., Gao, X., Wang, W., et al. (2020). *Clostridium perfringens* Beta2 Toxin Induced *In Vitro* Oxidative Damage and its Toxic Assessment in Porcine Small Intestinal Epithelial Cell Lines. *Gene* 759, 144999. doi:10.1016/j.gene.2020.144999
- Majumdar, A., Vainio, S., Kispert, A., McMahon, J., and McMahon, A. P. (2003). Wnt11 and Ret/Gdnf pathways Cooperate in Regulating Ureteric Branching during Metanephric Kidney Development. *Development* 130, 3175–3185. doi:10.1242/dev.00520
- Mayr, C. (2018). What Are 3' UTRs Doing? *Cold Spring Harb Perspect. Biol.* 11 (4), a034728–15. doi:10.1101/cshperspect.a034728
- Meng, J., Lu, Z., Liu, H., Zhang, L., Zhang, S., Chen, Y., et al. (2014). A Protocol for RNA Methylation Differential Analysis with MeRIP-Seq Data and exomePeak R/Bioconductor Package. *Methods* 69 (3), 274–281. doi:10.1016/j.ymeth.2014.06.008
- Meyer, K. D., Saletore, Y., Zumbo, P., Elemento, O., Mason, C. E., and Jaffrey, S. R. (2012). Comprehensive Analysis of mRNA Methylation Reveals Enrichment in 3' UTRs and Near Stop Codons. *Cell* 149 (7), 1635–1646. doi:10.1016/j.cell.2012.05.003
- Pandur, P., Lösche, M., Eisenberg, L. M., and Kühl, M. (2002). Wnt-11 Activation of a Non-canonical Wnt Signalling Pathway Is Required for Cardiogenesis. *Nature* 418, 636–641. doi:10.1038/nature00921
- Patil, D. P., Chen, C.-K., Pickering, B. F., Chow, A., Jackson, C., Guttman, M., et al. (2016). m⁶A RNA Methylation Promotes XIST-Mediated Transcriptional Repression. *Nature* 537 (7620), 369–373. doi:10.1038/nature19342
- Pertea, M., Pertea, G. M., Antonescu, C. M., Chang, T.-C., Mendell, J. T., and Salzberg, S. L. (2015). StringTie Enables Improved Reconstruction of a Transcriptome from RNA-Seq Reads. *Nat. Biotechnol.* 33 (3), 290–295. doi:10.1038/nbt.3122
- Robinson, J. T., Thorvaldsdóttir, H., Wenger, A. M., Zehir, A., and Mesirov, J. P. (2017). Variant Review with the Integrative Genomics Viewer. *Cancer Res.* 77 (21), e31–e34. doi:10.1158/0008-5472.CAN-17-0337
- Robinson, M. D., McCarthy, D. J., and Smyth, G. K. (2010). edgeR: a Bioconductor Package for Differential Expression Analysis of Digital Gene Expression Data. *Bioinformatics* 26 (1), 139–140. doi:10.1093/bioinformatics/btp616
- Sebastian-delaCruz, M., Olazagoitia-Garmendia, A., Gonzalez-Moro, I., Santin, I., Garcia-Etxebarria, K., and Castellanos-Rubio, A. (2020). Implication of m⁶A mRNA Methylation in Susceptibility to Inflammatory Bowel Disease. *Epigenomes* 4, 16. doi:10.3390/epigenomes4030016
- Shi, H., Wang, X., Lu, Z., Zhao, B. S., Ma, H., Hsu, P. J., et al. (2017). YTHDF3 Facilitates Translation and Decay of N⁶-Methyladenosine-Modified RNA. *Cell Res* 27 (3), 315–328. doi:10.1038/cr.2017.15
- Wang, X., Zhao, B. S., Roundtree, I. A., Lu, Z., Han, D., Ma, H., et al. (2015). N⁶-methyladenosine Modulates Messenger RNA Translation Efficiency. *Cell* 161 (6), 1388–1399. doi:10.1016/j.cell.2015.05.014
- Wang, Y., Sun, J., Lin, Z., Zhang, W., Wang, S., Wang, W., et al. (2020b). m⁶A mRNA Methylation Controls Functional Maturation in Neonatal Murine β-Cells. *Diabetes* 69 (8), 1708–1722. doi:10.2337/db19-0906
- Wang, Y., Zhang, L., Ren, H., Ma, L., Guo, J., Mao, D., et al. (2021). Role of Hakai in m⁶A Modification Pathway in *Drosophila*. *Nat. Commun.* 12 (1), 1–15. doi:10.1038/s41467-021-22424-51
- Wang, Y., Zheng, Y., Guo, D., Zhang, X., Guo, S., Hui, T., et al. (2020a). m⁶A Methylation Analysis of Differentially Expressed Genes in Skin Tissues of Coarse and Fine Type Liaoning Cashmere Goats. *Front. Genet.* 10, 1318. doi:10.3389/fgene.2019.01318

- Wu, C., Chen, W., He, J., Jin, S., Liu, Y., Yi, Y., et al. (2020). Interplay of m6A and H3K27 Trimethylation Restrains Inflammation during Bacterial Infection. *Sci. Adv.* 6 (34), eaba0647. doi:10.1126/sciadv.aba0647
- Xiao, W., Adhikari, S., Dahal, U., Chen, Y.-S., Hao, Y.-J., Sun, B.-F., et al. (2016). Nuclear M⁶A Reader YTHDC1 Regulates mRNA Splicing. *Mol. Cell* 61 (4), 507–519. doi:10.1016/j.molcel.2016.01.012
- Yang, J., Liu, J., Zhao, S., and Tian, F. (2020). N6-methyladenosine Mettl3 Modulates the Proliferation and Apoptosis of Lens Epithelial Cells in Diabetic Cataract. *Mol. Ther. - Nucleic Acids* 20, 111–116. doi:10.1016/j.omtn.2020.02.002
- Yu, G., Wang, L.-G., and He, Q.-Y. (2015). ChIPseeker: an R/Bioconductor Package for ChIP Peak Annotation, Comparison and Visualization. *Bioinformatics* 31 (14), 2382–2383. doi:10.1093/bioinformatics/btv145
- Zhao, T., Wang, J., Wu, Y., Han, L., Chen, J., Wei, Y., et al. (2021). Increased m6A Modification of RNA Methylation Related to the Inhibition of Demethylase FTO Contributes to MEHP-Induced Leydig Cell Injury☆. *Environ. Pollut.* 268 (115627), 115627–115637. doi:10.1016/j.envpol.2020.115627
- Zhao, X., Yang, Y., Sun, B.-F., Shi, Y., Yang, X., Xiao, W., et al. (2014). FTO-dependent Demethylation of N6-Methyladenosine Regulates mRNA Splicing and Is Required for Adipogenesis. *Cel Res* 24 (12), 1403–1419. doi:10.1038/cr.2014.151
- Zhou, Y., Liu, J., Lei, Q., Han, H., Liu, W., Cunwei, T., et al. (2020). Transcriptome Analysis of the Chicken Follicular Theca Cells with miR-135a-5p Suppressed. *G3 (Bethesda)* 10 (11), 4071–4081. doi:10.1534/g3.120.401701
- Zhu, T., Roundtree, I. A., Wang, P., Wang, X., Wang, L., Sun, C., et al. (2014). Crystal Structure of the YTH Domain of YTHDF2 Reveals Mechanism for Recognition of N6-Methyladenosine. *Cel Res* 24 (12), 1493–1496. doi:10.1038/cr.2014.152
- Zong, X., Zhao, J., Wang, H., and Wang, Y. (2018). PSXIV-41 Intestinal Inflammatory Impairs Lipid Transport via m6A-dependent Pathway. *J. Anim. Sci.* 96, 41–42. doi:10.1093/jas/sky404.093

Conflict of Interest: The authors declare that the research was conducted in the absence of any commercial or financial relationships that could be construed as a potential conflict of interest.

Publisher's Note: All claims expressed in this article are solely those of the authors and do not necessarily represent those of their affiliated organizations, or those of the publisher, the editors and the reviewers. Any product that may be evaluated in this article, or claim that may be made by its manufacturer, is not guaranteed or endorsed by the publisher.

Copyright © 2021 Zhang, Yang, Yang, Gao, Luo, Huang, Yan, Wang, Wang, Xie, Zhang and Gun. This is an open-access article distributed under the terms of the Creative Commons Attribution License (CC BY). The use, distribution or reproduction in other forums is permitted, provided the original author(s) and the copyright owner(s) are credited and that the original publication in this journal is cited, in accordance with accepted academic practice. No use, distribution or reproduction is permitted which does not comply with these terms.